https://doi.org/10.5194/acp-2019-838
Preprint. Discussion started: 28 November 2019

Atmospheric Chemistry and Physics Discussions

Insights on Atmospheric Oxidation Processes by Performing Factor Analyses on Sub-ranges of Mass Spectra

Yanjun Zhang[1], Otso Peräkylä[1], Chao Yan[1], Liine Heikkinen[1], Mikko Äijälä[1], Kaspar R. Daellenbach[1], Qiaozhi Zha[1], Matthieu Riva[1,2], Olga Garmash[1], Heikki Junninen[1,3], Pentti Paatero[1], Douglas Worsnop[1,4], and Mikael Ehn[1]

[1] Institute for Atmospheric and Earth System Research / Physics, Faculty of Science, University of Helsinki, Helsinki, 00014, Finland
[2] Univ Lyon, Université Claude Bernard Lyon 1, CNRS, IRCELYON, F-69626, Villeurbanne, France
[3] Institute of Physics, University of Tartu, Tartu, 50090, Estonia
[4] Aerodyne Research, Inc., Billerica, MA 01821, USA

Corresponding author: yanjun.zhang@helsinki.fi

Abstract

With the recent developments in mass spectrometry, combined with the strengths of factor analysis techniques, our understanding of atmospheric oxidation chemistry has improved significantly. The typical approach for using techniques like positive matrix factorization (PMF) is to input all measured data for the factorization in order to separate contributions from different sources and/or processes to the total measured signal. However, while this is a valid approach for assigning the total signal to factors, we have identified several cases where useful information can be lost if solely using this approach. For example, gaseous molecules emitted from the same source can show different temporal behaviors due differing loss terms, like condensation at different rates due to different molecular masses. This conflicts with one of PMF's basic assumptions of constant factor profiles. In addition, some ranges of a mass spectrum may contain useful information, despite contributing only minimal fraction to the total signal, in which case they are unlikely to have a significant impact on the factorization result. Finally, certain mass ranges may contain molecules formed via pathways not available to molecules in other mass ranges, e.g. dimeric species versus monomeric species. In this study, we attempted to address these challenges by dividing mass spectra into sub-ranges and applying the newly developed binPMF method to these ranges separately. We utilized a dataset from a chemical ionization atmospheric pressure interface time-of-flight (CI-APi-TOF) mass spectrometer as an example. We compare the results from these three different ranges, each corresponding to molecules of different volatilities, with binPMF results from the combined range. Separate analysis showed clear benefits in dividing factors for molecules of different volatilities more accurately, in

https://doi.org/10.5194/acp-2019-838
Preprint. Discussion started: 28 November 2019

Atmospheric Chemistry and Physics Discussions

resolving different chemical processes from different ranges, and in giving a chance for high-molecular-weight molecules with low signal intensities to be used to distinguish dimeric species with different formation pathways. In addition, daytime dimer formation (diurnal peak around noon) was identified, which may contribute to NPF in Hyytiälä. Also, dimers from NO_3 oxidation were separated by the sub-range binPMF, which would not be identified otherwise. We recommend PMF users to try running their analyses on selected sub-ranges in order to further explore their datasets.

1 Introduction

Huge amounts of volatile organic compounds (VOC) are emitted to the atmosphere every year (Guenther et al., 1995;Lamarque et al., 2010), which play a significant role in atmospheric chemistry and affect the oxidative ability of the atmosphere. The oxidation products of VOC can contribute to the formation and growth of secondary organic aerosols (Kulmala et al., 2013;Ehn et al., 2014;Kirkby et al., 2016;Troestl et al., 2016), affecting air quality, human health, and climate radiative forcing (Pope III et al., 2009;Stocker et al., 2013;Zhang et al., 2016;Shiraiwa et al., 2017). Thanks to the advancement in mass spectrometric applications, like the aerosol mass spectrometer (AMS) (Canagaratna et al., 2007) and chemical ionization mass spectrometry (CIMS) (Bertram et al., 2011;Jokinen et al., 2012;Lee et al., 2014) our capability to detect these oxidized products, as well as our understanding of the complicated atmospheric oxidation pathways in which they take part, have been greatly enhanced.

Monoterpenes ($C_{10}H_{16}$), one common group of VOC emitted in forested areas, have been shown to be a large source of atmospheric secondary organic aerosol (SOA). The oxidation of monoterpenes produces a wealth of different oxidation products (Oxygenated VOC, OVOC), including highly oxygenated organic molecules (HOM) with molar yields in the range of a few percent, depending on the specific monoterpene and oxidant (Ehn et al., 2014;Bianchi et al., 2019). Bianchi et al. (2019) summarized that HOM can be either Extremely Low Volatility Organic Compounds (ELVOC), Low Volatility Organic Compounds (LVOC), or Semi-volatile Organic Compounds (SVOC) (classifications by Donahue et al. 2012), depending on their exact structures. For less oxygenated products, the majority are likely to fall into the SVOC or the Intermediate VOC (IVOC) range. The volatility of the OVOC will determine their dynamics, including their ability to contribute to the formation of SOA and new particles (Bianchi et al., 2019;Buchholz et al., 2019).

The recent developments of CIMS techniques has allowed researchers to observe unprecedented numbers of OVOC, in real-time (Riva et al., 2019). This ability to measure thousands of compounds is a great benefit, but also a large challenge for the data analyst. For this reason, factor analytical techniques have often been applied to reduce the complexity of the data by finding co-varying signals

https://doi.org/10.5194/acp-2019-838
Preprint. Discussion started: 28 November 2019

Atmospheric Chemistry and Physics Discussions

that can be grouped into common factors (Huang et al., 1999). For aerosol and gas-phase mass spectrometry, positive matrix factorization, PMF (Paatero and Tapper, 1994;Zhang et al., 2011) has been the most utilized tool. The factors have then been attributed to sources (e.g. biomass burning organic aerosol) or processes (e.g. monoterpene ozonolysis) depending on the application and ability to identify spectral signatures (Yan et al., 2016;Zhang et al., 2017). In the vast majority of these PMF applications to mass spectra, the mass range of ions has been maximized in order to provide as much input as possible for the algorithm. This approach was certainly motivated in early application of PMF on e.g. offline filters, with chemical information of metals, water-soluble ions, and organic and elemental carbon (OC and EC), where the number of variables is counted in tens, and the number of samples in tens or hundreds (Zhang et al., 2017). However, with gas-phase CIMS, we often have up to a thousand variables, with hundreds or even thousands of samples, meaning that the amount of data itself is unlikely to be a limitation for PMF calculation. In this work, we aimed to explore potential benefits of dividing the spectra into sub-ranges before applying factorization analysis.

An inherent requirement of factorization approaches is that the factor profiles, in this case the relative abundancies of ions in the mass spectra, of each factor stay nearly constant. Due to the complexity and number of atmospheric processes affecting the formation, transformation, and loss of VOC, OVOC and aerosol, this often does not hold, and is one of the main limitations of factorization approaches. Given the different volatilities of OVOC, it may even be expected that molecules from the same source may have very different loss time scales, which may affect the factor analysis. Volatility issue has been studied and reported for AMS data, with different volatilities of various OA types (Huffman et al., 2009;Crippa et al., 2014;Paciga et al., 2016;Äijälä et al., 2017). Semi-volatile oxygenated organic aerosol (SV-OOA) and Low-volatility oxygenated organic aerosol (LV-OOA) can both be mainly produced from biogenic sources, but get separated based on different volatilities by PMF (El Haddad et al., 2013). Sekimoto et al. (2018) found that the two profiles resolved with VOC emitted from biomass burning had different estimated volatilities. As the volatility of a molecule is linked to its molecular mass (Peräkylä et al., 2019), it may be beneficial to apply PMF separately to mass ranges where one can expect the loss processes to be similar, thereby resulting in more constant factor profiles. In this way, distinct sources are hopefully separated by PMF, with minimized influence of differing volatilities from one source.

The number of PMF or other factorization studies utilizing CIMS data remains very limited. “Traditional” PMF analyses have so far, to our knowledge, only been applied to nitrate-based chemical ionization atmospheric pressure interface time-of-flight (CI-APi-TOF) data (Yan et al., 2016;Massoli et al., 2018). One study has also utilized non-negative matrix factorization (NNMF) to look at diurnal trends of Iodide ToF-CIMS data (Lee et al., 2018). The lack of more studies utilizing

https://doi.org/10.5194/acp-2019-838
Preprint. Discussion started: 28 November 2019

Atmospheric Chemistry and Physics Discussions

PMF, or other factorization techniques, on CIMS data is likely partly due to the complexity of the data, with multiple overlapping ions hampering HR peak fitting (Zhang et al., 2019). In addition, variable factor profiles may hamper PMF's ability to correctly separate the factors. The two CI-APi-TOF studies utilized the nearly the entire measured spectrum (from around 200 Th to around 600 Th), either in unit mass resolution (UMR) or high resolution (HR) peak fitting data (Yan et al., 2016;Massoli et al., 2018). Massoli et al. (2018) estimated the volatility of the molecules they detected, finding that all the six extracted factors had notable contributions from IVOC, SVOC and (E)LVOC. These compound groups will have clearly different loss mechanisms, and thereby loss rates, suggesting that variation in factor profiles is inevitable, even if the source was identical for all molecules in the factor. We hypothesize that this effect further hampers the correct factorization, and further that this effect can be reduced by dividing the spectra into separate ranges, with each sub-range containing molecules with roughly similar loss mechanisms and rates.

As an additional motivation to separate different ranges from the mass spectrum, it is not only the loss mechanisms, but also the formation pathways that may differ. For example, atmospheric oxidation chemistry of organics is, to a large extent, the chemistry of peroxy radicals (RO_2) (Orlando and Tyndall, 2012).These RO_2 are initiated by VOC reacting with oxidants like ozone, or the hydroxyl (OH) or nitrate (NO_3) radicals, while their termination occurs mainly by bimolecular reactions with NO, HO_2 and/or other RO_2. Some product molecules can be formed from many of the three termination pathways, while for example ROOR "dimers" can only be formed from RO_2+RO_2 reactions (Berndt et al., 2018a;Berndt et al., 2018b). This also means that there can be six different pathways to form dimers from the same precursors VOC, by combining RO_2 formed from the same or different oxidants. As an example of the latter, an ROOR dimer can contain one moiety produced from ozone oxidation and another moiety from NO_3 oxidation (Yan et al., 2016). Thus, their concentration is dependent on both the precursor VOC concentration, and the concentrations of both oxidants. Such a molecule will not have a direct equivalent in any of the monomer products, dependent on only one oxidant, which again may complicate the separation of such factors by PMF, if the entire spectrum is analyzed once. However, if separating the monomer and dimer products before PMF analysis, separation of different formation pathways can potentially become simpler.

Recently, we proposed a new PMF approach, binPMF, to simplify the analysis of mass spectral data (Zhang et al., 2019). This method divides the mass spectrum into narrow bins, typically some tens of bins per integer mass, depending on the mass resolving power of the instrument, before performing PMF analyses. In this way, binPMF does not require any time-consuming, and potentially subjective high resolution peak fitting, and can thus be utilized for data exploration at a very early stage of data analysis. Data preparation is nearly as simple as in the case of UMR analysis, yet it utilizes much

https://doi.org/10.5194/acp-2019-838
Preprint. Discussion started: 28 November 2019

Atmospheric Chemistry and Physics Discussions

more spectral information as it does not sum up signal over all ions at each integer mass. In addition to saving time and effort in data analysis, the results are less sensitive to mass calibration fluctuations. Finally, the binning also greatly increases the number of input variables, which has the advantage that factor analysis with smaller mass ranges becomes more feasible, as more meaningful variation is supplied to the algorithm.

We designed this study to explore the benefits of separate analysis of different mass ranges from mass spectra. We used a previously published ambient dataset measured by a CI-APi-TOF, and conducted binPMF analysis with three different mass ranges, roughly corresponding to different volatility ranges. We compared the results from the sub-range analyses with each other and with results from binPMF run on the combined ranges. We found that more meaningful factors are separated from our dataset by utilizing the sub-ranges, and believe that this study will provide new perspectives for future studies analyzing gas-phase CIMS data.

2 Methodology

The focus of this work is on retrieving new information from mass spectra by applying new analytical approaches. Therefore, we chose a dataset that has been presented earlier, though without PMF analysis, by Zha et al. (2018), and was also used in the first study describing the binPMF method (Zhang et al., 2019). The measurements are described in more details below in section 2.1, while the data analysis techniques used in this work are presented in section 2.2.

2.1 Measurements

2.1.1 Ambient site

The ambient measurements were conducted at the Station for Measuring Ecosystem–Atmosphere Relations (SMEAR) II in Finland (Hari and Kulmala, 2005) as part of the Influence of Biosphere-Atmosphere Interactions on the Reactive Nitrogen budget (IBAIRN) campaign (Zha et al, 2018). Located in the boreal environment in Hyytiälä, SMEAR II is surrounded with coniferous forest and has limited anthropogenic emission sources nearby. Diverse measurements of meteorology, aerosol and gas phase properties are continuously conducted at the station. Details about the meteorological conditions and temporal variations of trace gases during IBAIRN campaign are presented by Zha et al. (2018) and Liebmann et al. (2018).

2.1.2 Instrument and data

Data were collected with a nitrate (NO_3^-)-based chemical ionization atmospheric pressure interface time-of-flight mass spectrometer (CI-APi-TOF, Jokinen et al., 2012) with about 4000 Th Th^{-1} mass resolving power, at ground level in September, 2016. In our study, the mass spectra were averaged to 1 h time resolution from September 6th to 22nd for further analysis. We use the thomson (Th) as the

https://doi.org/10.5194/acp-2019-838
Preprint. Discussion started: 28 November 2019

Atmospheric Chemistry and Physics Discussions

unit for mass/charge, with 1 Th = 1 Da/e, where *e* is the elementary charge. As all the data discussed in this work are based on negative ion mass spectrometry, we will use the absolute value of the mass/charge, although the charge of each ion will be negative. The masses discussed in this work includes the contribution from the nitrate ion, 62, unless specifically mentioned. Furthermore, as the technique is based on soft ionization with NO_3^- ions, any multiple charging effects are unlikely, and therefore the reported mass/charge values in thomson can be considered equivalent to the mass of the ion in Da.

The forest site of Hyytiälä is dominated by monoterpene emissions (Hakola et al., 2006). The main feature of previous CI-APi-TOF measurements in Hyytiälä (Ehn et al., 2014;Yan et al., 2016) has been a bimodal distributions of HOM, termed monomers and dimers, as they are formed of either one or two RO_2 radicals, respectively. For the analysis in this study, we chose three mass/charge (*m/z*) ranges of 50 Th each (Figure 1), corresponding to regions between which we expect differences in formation or loss mechanisms. In addition to regions with HOM monomers and HOM dimers, one range was chosen at lower masses, in a region presumably mainly consisting of molecules that are less likely to condense onto aerosol particles (Peräkylä et al., 2019).

2.2 Positive matrix factorization (PMF)

After the model of PMF was developed (Paatero and Tapper, 1994), numerous applications have been conducted with different types of environmental data (Song et al., 2007;Ulbrich et al., 2009;Yan et al., 2016;Zhang et al., 2017). By reducing dimensionality of the measured dataset, PMF model greatly simplifies the data analysis process with no requirement for prior knowledge of sources or pathways as essential input. The main factors can be further interpreted with their unique/dominant markers (elements or masses).

The basic assumption for PMF modelling is mass balance, which assumes that ambient concentration of a chemical component is the sum of contributions from several sources or processes, as shown in equation (1).

$$\mathbf{X} = \mathbf{TS} \times \mathbf{MS} + \mathbf{R} \quad (1)$$

In equation (1), **X** stands for the time series of measured concentration of different variables (*m/z* in our case), **TS** represents the temporal variation of factor contributions, **MS** stands for factor profiles (mass spectral profiles), and **R** is the residual as the difference of the modelled and the observed data. The matrices **TS** and **MS** are iteratively calculated by a least-squares algorithm utilizing uncertainty estimates, to pursue minimized Q value as shown in equation (2), where S_{ij} is the estimated uncertainty, an essential input in PMF model.

$$Q = \sum\sum\left(\frac{R_{ij}}{S_{ij}}\right)^2 \quad (2)$$

https://doi.org/10.5194/acp-2019-838
Preprint. Discussion started: 28 November 2019

Atmospheric Chemistry and Physics Discussions

PMF model was conducted by multi-linear engine (ME-2) (Paatero, 1999) interfaced with Source Finder (SoFi, v6.3) (Canonaco et al., 2013). Signal-to-noise ratio (SNR) was calculated as SNR*ij* = abs (*Xij*) / abs (*Sij*). When the Signal-to-noise ratio (SNR) is below 1, the signal of X_{ij} will be down-weighted by replacing the corresponding uncertainty S_{ij} by S_{ij}/SNR$_{ij}$ (Visser et al., 2015). Future studies should pay attention to the potential risk when utilizing this method since down-weighting low signals element-wise will create a positive bias to the data. Robust mode was operated in the PMF modelling, where outliers ($\left|\frac{R_{ij}}{S_{ij}}\right| > 4$) were significantly down-weighted (Paatero, 1997).

2.3 binPMF

As a newly developed application of PMF for mass spectral data, binPMF has no requirement for chemical composition information, while still taking advantage of the HR mass spectra, saving effort and time (Zhang et al., 2019). To explore the benefits of analyzing separated mass ranges, we applied binPMF to the three separated ranges. The three ranges were also later combined for binPMF analysis as comparison with the previous results. The PMF model requires both data matrix and error matrix as input, and details of the preparation of data and error matrices are described below.

2.3.1 Data matrix

Different from normal UMR or HR peak fitting, in binPMF, the mass spectra are divided into small bins after baseline subtraction and mass axis calibration. Linear interpolation was first conducted to the mass spectra with a mass interval of 0.001 Th. Then the interpolated data was averaged into bins of 0.02 Th width. We selected three ranges for further analysis based on earlier studies (Ehn et al., 2014;Yan et al., 2016;Bianchi et al., 2019;Peräkylä et al., 2019).

- Range 1, *m/z* 250 – 300 Th, 51 unit masses × 25 bins per unit mass = 1275 bins/variables, consisting mainly of molecules with five to nine carbon atoms and four to nine oxygen atoms in our dataset.
- Range 2, *m/z* 300 – 350 Th, 51×25 = 1275 bins, mainly corresponding to HOM monomer products, featured with nine to ten C- and seven to ten O-atoms.
- Range 3, *m/z* 510 – 560 Th, 51×30 = 1530 bins, mainly corresponding to HOM dimer products, with carbon numbers of sixteen to twenty and eleven to fifteen O-atoms.

For a nominal mass *N*, the signal region included in further analyses was between *N*-0.2 Th and *N*+0.3 Th for Range 1 and 2, and between *N*-0.2 Th and *N*+0.4 Th for Range 3. The data were averaged into 1-h time resolution and in total we had 384 time points in the data matrix.

2.3.2 Error matrix

https://doi.org/10.5194/acp-2019-838
Preprint. Discussion started: 28 November 2019

Atmospheric Chemistry and Physics Discussions

The error matrix represents the estimated uncertainty for each element of the data matrix and is crucial for iterative calculation of the Q minimum. Equation (3) is used for error estimation (Polissar et al., 1998),

$$S_{ij} = \sigma_{ij} + \sigma_{\text{noise}} \quad (3)$$

where S_{ij} represents the uncertainty of m/z j at time i, σ_{ij} stands for counting statistics uncertainty and is estimated as follows,

$$\sigma_{ij} = a \times \frac{\sqrt{I_{ij}}}{\sqrt{t_s}} \quad (4)$$

where I is the signal intensity term, in unit of counts per second (cps), t_s stands for length of averaging in seconds, while a is an empirical coefficient to compensate for unaccounted uncertainties (Allan et al., 2003;Yan et al., 2016) and is 1.28 in our study as previously estimated from laboratory experiments (Yan et al., 2016). The σ_{noise} term was estimated as the median of the standard deviations from signals in the bins in the region between nominal masses, where no physically meaningful signals are expected.

3 Results

3.1 General overview of the dataset/spectrum

During the campaign, in autumn, 2016, the weather was overall sunny and humid with average temperature of 10.8 ℃ and relative humidity (RH) of 87% (Zha et al., 2019). The average concentration of NO_x and O_3 was 0.4 ppbv and 21 ppbv, respectively. The average total HOM concentration was ~ 10^8 molecules cm^{-3}.

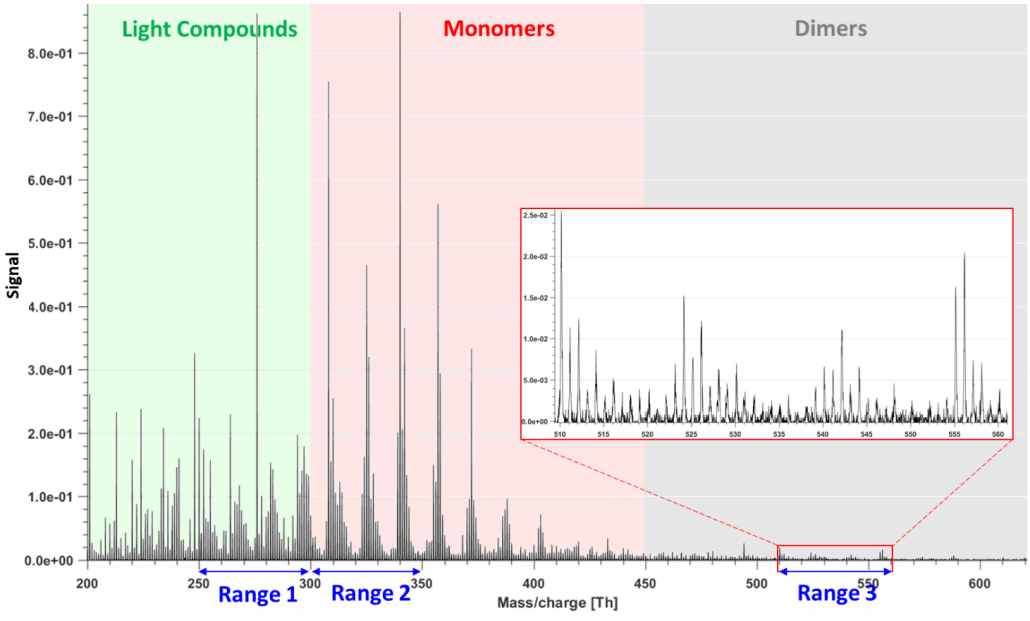

https://doi.org/10.5194/acp-2019-838
Preprint. Discussion started: 28 November 2019


Atmospheric Chemistry and Physics Discussions

Figure 1. Example of mass spectrum with 1-h time resolution measured from a boreal forest environment during the IBAIRN campaign (at 18:00, Finnish local time, UTC+2). The mass spectrum was divided into three parts and three sub-ranges were chosen from different parts for further analysis in our study. The nitrate ion (62 Th) is included in the mass.

Figure 1 shows the 1 h averaged mass spectrum taken at 18:00 on September 12, as an example of the analyzed dataset. In addition to exploring the benefits of this type of sub-range analysis in relation to different formation or loss pathways, separating into sub-ranges may also aid factor identification for low-signal regions. As shown in Figure 1, there is a difference of 1-2 orders of magnitude in the signal intensity between Range 3 and Ranges 1-2. If all Ranges are run together, we would expect that the higher signals from Ranges 1 and 2 will drive the factorization. While if run separately, separating formation pathways of dimers in Range 3 will likely be easier. As dimers have been shown to be crucial for the formation of new aerosol particles from monoterpene oxidation (Kirkby et al., 2016;Troestl et al., 2016;Lehtipalo et al., 2018), this information may even be the most critical in some cases, despite the low contribution of these peaks to the total measured signal.

binPMF was separately applied to Range 1, 2, 3, and a 'Range combined' which comprised all the three sub-ranges. All the PMF runs for the four ranges were conducted from two to ten factors and repeated three times for each factor number, to assure the consistency of the results. Factorization results and evolution with increasing factor number are briefly described in the following sections, separately for each Range (sections 3.2 – 3.5). More detailed discussion and comparison between the results are presented in Section 4.

3.2 binPMF on Range 1 (250 – 300 Th)

As has become routine (Zhang et al., 2011;Craven et al., 2012), we first examined the mathematical parameters of our solutions. From two to ten factors, Q/Q_{exp} decreased from 2.8 to 0.7 (Fig S1 in supplementary information), and after three factors, the decreasing trend was gradually slowing down and approaching one, which is the ideal value for Q/Q_{exp} as a diagnostic parameter. The unexplained variation showed a decline from 18% to 8% from two to ten factors.

In the two-factor results, two daytime factors were separated, with peak time both at 14:00 - 15:00. One factor was characterized by large signals at 250 Th, 255 Th, 264 Th, 281 Th, 283 Th, 295 Th, 297 Th. The other factor was characterized by large signals at 294 Th, 250 Th, 252 Th, 264 Th, 266 Th, 268 Th, and 297 Th. In Hyytiälä, as reported in previous studies, odd masses observed by the nitrate CI-APi-TOF are generally linked to monoterpene-derived organonitrates during the day (Ehn et al., 2014;Yan et al., 2016). When the factor number increased to three, the two earlier daytime factors remained similar with the previous result, while a new factor appeared with a distinct sawtooth shape in the diurnal cycle. The main marker in the spectral profile was 276 Th, with a clear negative

https://doi.org/10.5194/acp-2019-838
Preprint. Discussion started: 28 November 2019

Atmospheric Chemistry and Physics Discussions

mass defect. When one more factor was added, the previous three factors remained similar as in the three-factor solution, and a new morning factor was resolved, with 264 Th and 297 Th dominant in the mass spectral profile, and a diurnal peak at 11:00.

As the factor number was increased, more daytime factors were separated, with similar spectral profiles to existing daytime factors and various peak times. No nighttime factors were found in the analysis even when the factor number reached ten. We chose the four-factor result for further discussion, and Figure 2 shows the result of Range 1, with spectral profile, time series, diurnal cycle and factor contribution. As shown in Figure 2d, Factors 1-3 are all daytime factors, while Factor 4 has a sawtooth shape, which is caused by contamination, mainly by perfluorinated acids, of the inlet's automated zeroing every three hours during the measurements (Zhang et al., 2019). The zeroing periods have been removed from the dataset before binPMF analysis, but the contamination factor was still resolved. This factor is discussed in more detail in sections 4.1.1 and 4.1.4.

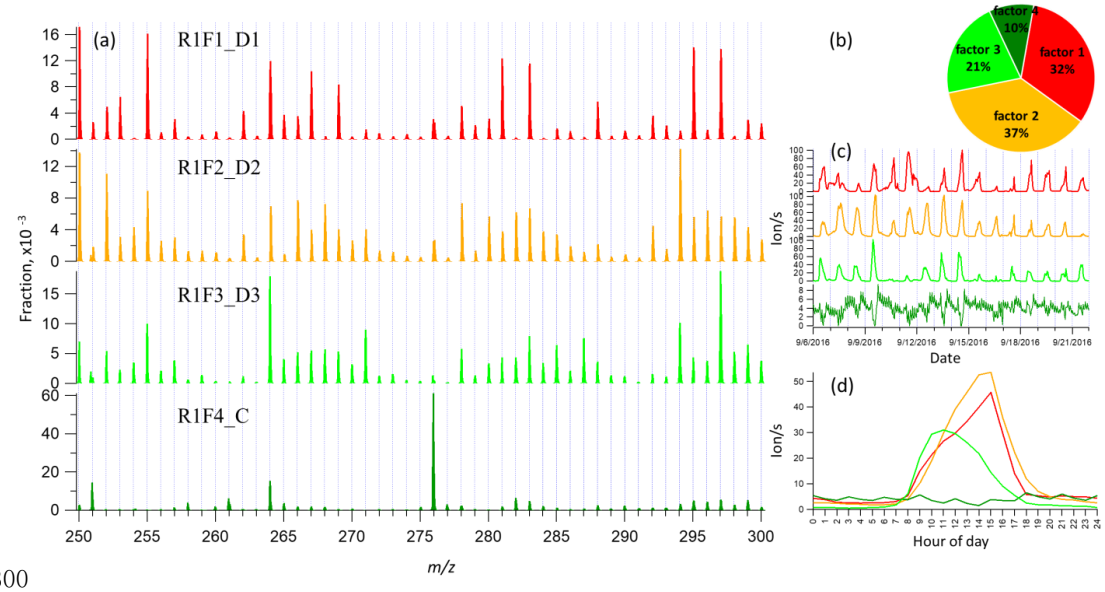

Figure 2 Four-factor result for Range 1, for (a) factor spectral profiles, (b) factor contribution, (c) time series and (d) diurnal trend. Details on the factors' naming schemes are shown in Table 1.

3.3 binPMF on Range 2 (300-350 Th)

This range covers the monoterpene HOM monomer range, and binPMF results have already been discussed by Zhang et al. (2019) as a first example of the application of binPMF on ambient data. Our input data here is slightly different. In the previous study, the 10 min automatic zeroing every three hours was not removed before averaging to 1 hour time resolution while here, we have removed this data. Overall, the results are similar as in our earlier study, and therefore the result are just briefly

https://doi.org/10.5194/acp-2019-838
Preprint. Discussion started: 28 November 2019

Atmospheric Chemistry and Physics Discussions

summarized below for further comparison and discussion in Section 4. Similar to Range 1, both the Q/Q_{exp} (2.2 to 0.6) and unexplained variation (16% to 8%) declined with the increased factor number from two to ten.

When the factor number was two, one daytime and one nighttime factor were separated, with diurnal peak times at 14:00 and 17:00, respectively. The nighttime factor was characterized by masses at 340 Th, 308 Th and 325 Th (monoterpene ozonolysis HOM monomers (Ehn et al., 2014)) and remained stable throughout the factor evolution from two to ten factors. With the addition of more factors, no more nighttime factors got separated while the daytime factor was further separated and more daytime factors appeared, peaking at various times in the morning (10:00 am), at noon or in the early afternoon (around 14:00 pm and 15:00 pm). High contribution of 339 Th can be found in all the daytime factor profiles. As the factor number reached six, a contamination factor appeared, characterized by large signals at 339 Th and 324 Th, showing negative mass defects (Figure S2 in the Supplement). The factor profile is nearly identical to the contamination factor determined in Zhang et al. (2019), where the zeroing periods were not removed, causing larger signals for the contaminants. In our dataset, where the zeroing periods were removed, no sawtooth pattern was discernible in the diurnal trend, yet it could still be separated even though it only contributed 3% to Range 2. More about the contamination factors from different ranges will be discussed in Section 4.1.4. Since the aim of this study is mainly to explore the benefits of analyzing different ranges of the mass spectrum, we chose to show the four-factor result below, to simplify the later discussion and comparison. Figure 3 shows four-factor result of Range 2, with spectral profile, time series, diurnal cycle and factor contribution.

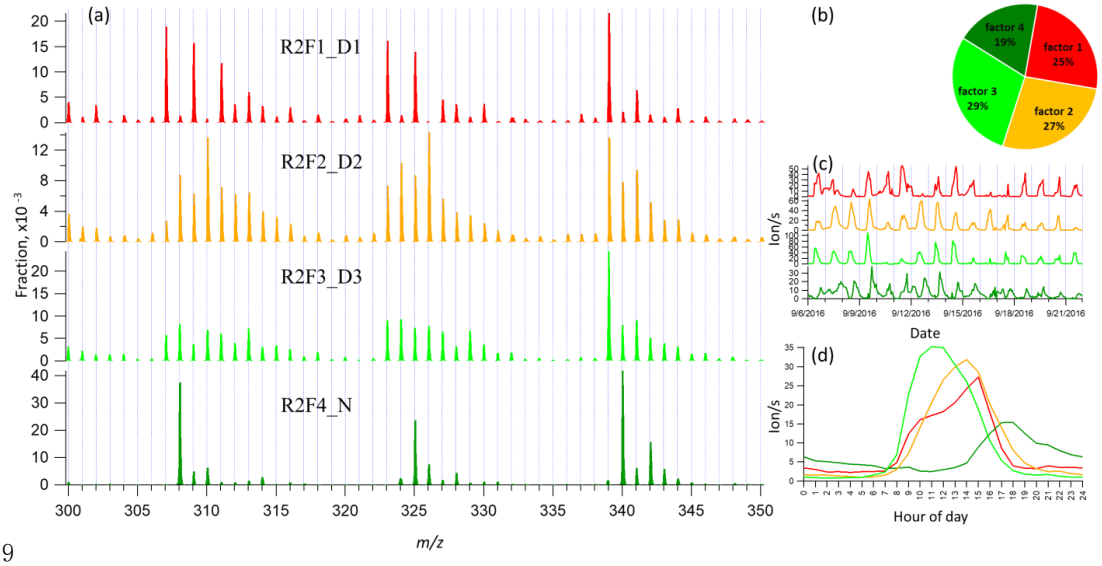

https://doi.org/10.5194/acp-2019-838
Preprint. Discussion started: 28 November 2019

Atmospheric Chemistry and Physics Discussions

Figure 3 Four-factor result for Range 2, for (a) factor spectral profiles, (b) factor contribution, (c) time series and (d) diurnal trend. Details on the factors' naming schemes are shown in Table 1.

3.4 binPMF on Range 3 (510-560 Th)

Range 3 represents mainly the monoterpene HOM dimers (Ehn et al., 2014). Similar to Range 1 and 2, both the Q/Q_{exp} (1.5 to 0.6) and unexplained variation (18% to 15%) showed decreasing trend with the increased factor number (2-10). As can be seen from Figure 1, data in Range 3 had much lower signals, compared to that of the Range 1 and 2, explaining the higher unexplained variation for Range 3.

In the two-factor result for Range 3, one daytime and one nighttime factor appeared, with diurnal peak times at noon and 18:00, respectively. The nighttime factor was characterized by ions at 510 Th, 524 Th, 526 Th, 542 Th, and 555 Th, 556 Th, while the daytime factor showed no dominant marker masses, yet with relatively high signals at 516 Th, 518 Th and 520 Th. As the number of factors increased to three, one factor with almost flat diurnal trend was separated, with dominant masses of 510 Th, 529 Th, 558 Th. Most peaks in this factor had negative mass defects, and this factor was again linked to a contamination factor. The four-factor result resolved another nighttime factor with a dominant peak at 555 Th, and effectively zero contribution during daytime. As the factor number was further increased, the new factors seemed like splits from previous factors with similar spectral profiles. We therefore chose four-factor result also for Range 3 (results shown in Fig. 4) for further discussion.

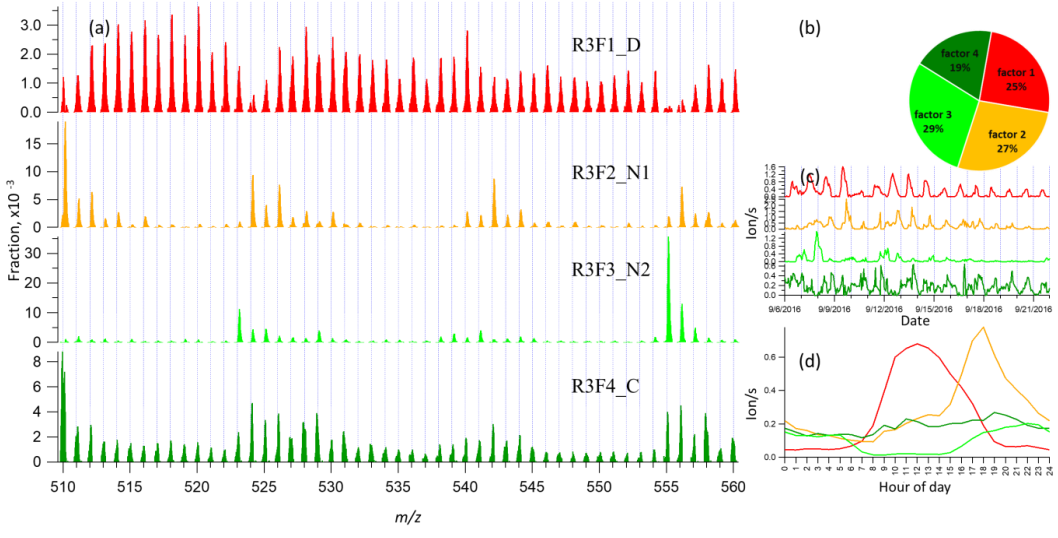

Figure 4 Four-factor result for Range 3, for (a) factor spectral profiles, (b) factor contribution, (c) time series and (d) diurnal trend. Details on the factors' naming schemes are shown in Table 1.

https://doi.org/10.5194/acp-2019-838
Preprint. Discussion started: 28 November 2019

Atmospheric Chemistry and Physics Discussions

352 3.5 binPMF on Range Combined (250-350 Th & 510-560 Th)

353 As comparison to the previous three ranges, we conducted the binPMF analysis on Range Combined,
354 which is the combination of the three ranges. The results of this range are fairly similar to those of
355 Ranges 1 and 2, as could be expected since the signal intensities in these ranges were much higher
356 than in Range 3. As the number of factors increased (2-10), both the Q/Q_{exp} (1.3 to 0.6) and
357 unexplained variation (16% to 8%) showed a decreasing trend.

358 In the two-factor result, one daytime factor and one nighttime factor were separated. In the nighttime
359 factor, most masses were found at even masses, and the fraction of masses in Range 3 was much
360 higher than that in daytime factor. In contrast, in the daytime factor, most masses were observed at
361 odd masses and the fraction of signal in Range 3 was much lower. During the day, photochemical
362 reactions increase the concentration of NO, which serves as peroxy radical (RO_2) terminator and often
363 outcompetes RO_2 cross reactions in which dimers can be formed (Ehn et al., 2014). Thus, the
364 production of dimers is suppressed during the day, yielding instead a larger fraction of organic nitrates,
365 as has been shown also previously (Yan et al., 2016).

366 With the increase of the number of factors, more daytime factors were resolved with different peak
367 times. When the factor number reached seven, a clear sawtooth-shape diurnal cycle occurred, i.e. the
368 contamination factor, caused by the zeroing. As more factors were added, no further nighttime factors
369 were separated, and only more daytime factors appeared. To simplify the discussion and inter-range
370 comparison, we also here chose the four-factor result for further analysis, as it already provided
371 enough information for our main goal in this study. Figure 5 shows the four-factor result of Range
372 Combined, with spectral profile, time series, diurnal cycle and factor contribution. The signals in
373 range of 510-560 Th were enlarged 100-fold to be visible.

https://doi.org/10.5194/acp-2019-838
Preprint. Discussion started: 28 November 2019

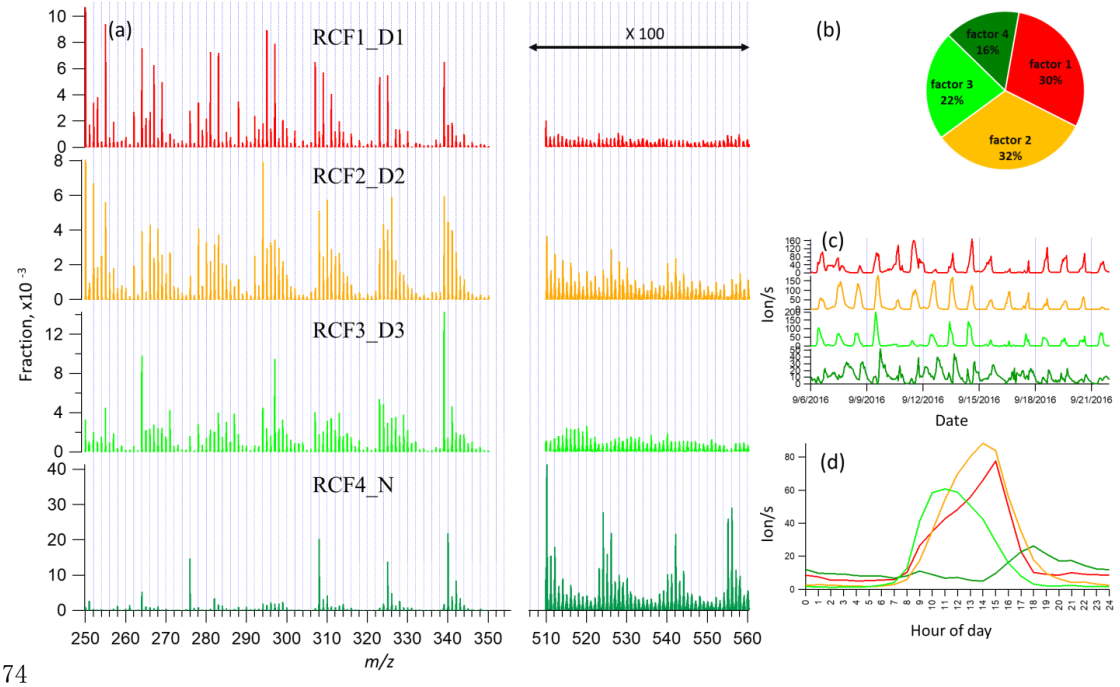

Figure 5 Four-factor result for Range Combined, for (a) factor spectral profiles, (b) factor contribution, (c) time series and (d) diurnal trend. Details on the factors' naming schemes are shown in Table 1.

4 Discussion

In Section 3, results by binPMF analysis were shown for Ranges 1, 2, 3 and Combined. In this section, we discuss and compare the results from the different ranges. To simplify the inter-range comparison, we chose four-factor results for all the four ranges, with the abbreviations shown in Table 1. From Range 1, three daytime factors and a contaminations factor were separated. In Range 2, three daytime factors and one nighttime factor (abbreviated as R2F4_N) were resolved. The R2F4_N factor was characterized by signals at 308 Th ($C_{10}H_{14}O_7 \cdot NO_3^-$), 325 Th ($C_{10}H_{15}O_8 \cdot NO_3^-$), and 340 Th ($C_{10}H_{14}O_9 \cdot NO_3^-$), and can be confirmed as monoterpene ozonolysis products (Ehn et al., 2014;Yan et al., 2016). With the increase of factor number to six, the contamination factor got separated also in this mass range. In Range 3, one daytime factor, two nighttime factors and a contamination factor were separated. The first nighttime factor (R3F2_N1) had large peaks at 510 Th ($C_{20}H_{32}O_{11} \cdot NO_3^-$) and 556 Th ($C_{20}H_{30}O_{14} \cdot NO_3^-$), dimer products that have been identified during chamber studies of monoterpene ozonolysis (Ehn et al., 2014). The molecule observed at 510 Th has 32 H-atoms, suggesting that one of the RO_2 involved would have been initiated by OH, which is formed during the ozonolysis of alkenes such as monoterpenes at nighttime (Atkinson et al., 1992;Paulson and

https://doi.org/10.5194/acp-2019-838
Preprint. Discussion started: 28 November 2019

Atmospheric Chemistry and Physics Discussions

393 Orlando, 1996). The other nighttime factor (R3F3_N2) was dominated by ions at 523 Th
394 ($C_{20}H_{31}O_8NO_3{\cdot}NO_3^-$) and 555 Th ($C_{20}H_{31}O_{10}NO_3{\cdot}NO_3^-$), representing nighttime monoterpene
395 oxidation involving NO_3. As these dimers contain only one N-atom, and 31 H-atoms, we can assume
396 that they are formed from reactions between an RO_2 formed from NO_3 oxidation and another RO_2
397 formed by ozone oxidation. These results match well with the profiles in a previous study by Yan et
398 al. (2016). The results of Range Combined are very similar to Range 2, with one nighttime factor and
399 three daytime factors. The contamination factor was separated with increase of factor number to seven.
400
401 Table 1. Summary of PMF results for the different mass ranges

Range	Factor number	Factor name[a]	Dominant peaks	Peak time
1 (250 - 300 Th)	1	R1F1_D1	250, 255, 295, 297	15:00
	2	R1F2_D2	250, 252, 294	15:00
	3	R1F3_D3	264, 297	11:00
	4	R1F4_C	276	-[b]
2 (300 - 350 Th)	1	R2F1_D1	307, 309, 323, 325, 339,	15:00
	2	R2F2_D2	310, 326, 339,	14:00
	3	R2F3_D3	339	11:00
	4	R2F4_N	308, 325, 340	18:00
3 (510 – 560 Th)	1	R3F1_D	516, 518, 520, 528, 540	12:00
	2	R3F2_N1	510, 524, 542, 556	18:00
	3	R3F3_N2	523, 555	22:00
	4	R3F4_C	510, 558	-[b]
Combined (1, 2, 3)	1	RCF1_D1	250, 255, 295, 339	15:00
	2	RCF2_D2	250, 252, 294, 339	14:00
	3	RCF3_D3	264, 297, 339	11:00
	4	RCF4_N	308, 340, 510, 524, 555, 556	18:00

402 [a] Factor name is defined with range name, factor number and name. For example, RxFy represents Factor y in Range x.
403 RC stands for Range Combined. For the factor name, D is short for daytime, N for Nighttime, C for contamination.
404 [b] The contamination factor in Range 1 shows sawtooth pattern; while in Range 3 shows no diurnal pattern.
405

406 4.1 Comparison of different ranges

407 4.1.1 Time series correlation

408 In Figure 6, the upper panels show the time series correlations among the first three ranges. As
409 expected based on the results above, generally the daytime factors, and the two nighttime
410 monoterpene ozonolysis factors (R2F4_N and R3F2_N1) correlated well, respectively. However, the
411 contamination factors did now show strong correlation between different ranges, even though
412 undoubtedly from the same source. More about the contamination factors will be discussed in Section
413 4.1.4. The lower panels in Figure 6 displays the correlations between the first three ranges and the
414 Range Combined, and clearly demonstrates that the results of Range Combined is mainly controlled
415 by high signals from Range 1 and 2. More detailed aspects of the comparison between factors in

https://doi.org/10.5194/acp-2019-838
Preprint. Discussion started: 28 November 2019

Atmospheric Chemistry and Physics Discussions

different ranges is given in the following sections. The good agreements between factors from different subranges also help to verify the robustness of the solutions.

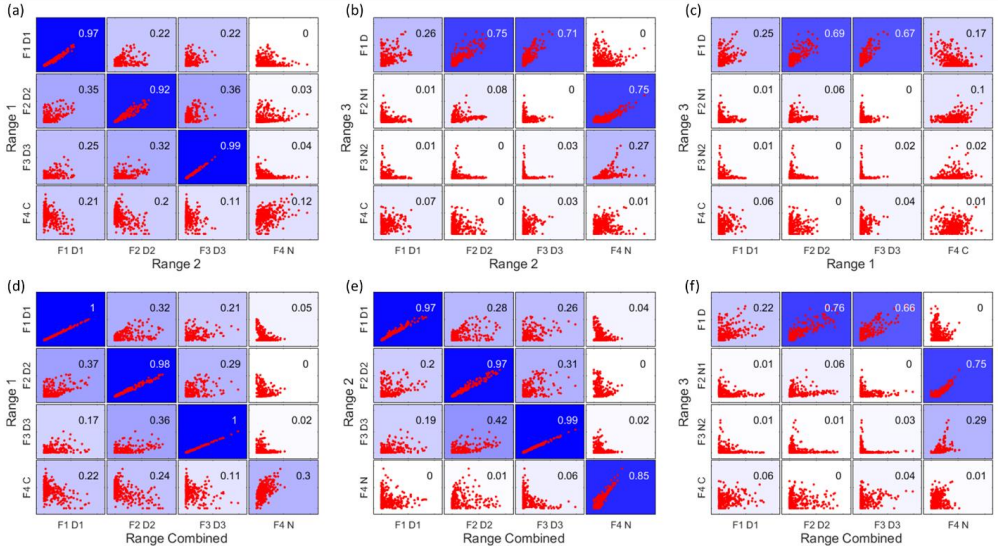

Figure 6 Time series correlations among Range 1, 2, 3 (upper panels a-c), and between the first three ranges and the Range Combined (lower panels d-f). The abbreviations for different factors are the same in Table 1, with F for factor, D for daytime, N for nighttime and C for contamination, e.g. F1D1 for Factor 1 daytime 1. The coefficient of determination, R^2, is marked in each subplot by a number shown in the right upper corners and by the blue colors, with stronger blue indicating higher R^2.

4.1.2 Daytime factor comparison

As mentioned above, with increasing number of factors, usually more daytime factors will be resolved, reflecting the complicated daytime photochemistry. The three daytime factors between Range 1 and 2 agreed with each other quite well (Figure 6a). However, R1F1_D1 and R2F1_D1 did not show strong correlation with the only daytime factor in Range 3 (R3F1_D), while the other two daytime factors in both Range 1 and 2, i.e. R1F2_D2, R1F3_D3, R2F2_D2, R2F3_D3, correlated well with R3F1_D from Range 3.

The 1st daytime factors from Range 1 and 2, R1F1_D1 and R2F1_D1, were mainly characterized by odd masses 255 Th, 281 Th, 283 Th, 295 Th, 297 Th, 307 Th, 309 Th, 311 Th, 323 Th, 325 Th, 339 Th. The factors are dominated by organonitrates. Organic nitrate formation during daytime is generally associated with the termination of RO_2 radicals by NO. This termination step is mutually exclusive with the termination of RO_2 with other RO_2, leading to dimer formation. If the NO concentration is the limiting factor for the formation of these factors, the low correlations between the NO-terminated monomer factors, and the dimer factors, is to be expected. In contrast, if the other

https://doi.org/10.5194/acp-2019-838
Preprint. Discussion started: 28 November 2019


Atmospheric Chemistry and Physics Discussions

438 daytime factors mainly depend on oxidant and monoterpene concentrations, some correlation
439 between those, and the daytime dimer factor, is to be expected, as shown in Figure 6b, c.
440 All the spectral profiles resolved from Range Combined binPMF analysis inevitably contained mass
441 contribution from 510 – 560 Th, even the daytime factor from Range Combined (RCF1_D1) which
442 did not show clear correlation with R3F1_D from Range 3 (Figure 6e).
443 The 2nd and 3rd daytime factors in Range 1 and 2, R1F2_D2, R1F3_D3, R2F2_D2, R2F3_D3, had
444 high correlations with R3F1_D in Range 3. Daytime factors in Range Combined (RCF2_D2 and
445 RCF3_D3) also showed good correlation with R3F1_D in Range 3. However, if we compare R3F1_D
446 and the mass range of 510 – 560 Th of the daytime factors in Range Combined, just with a quick look,
447 we can readily see the difference. The daytime factor separated in Range 3 (R3F1_D) basically has
448 no obvious markers in the profile, and as mentioned above, up to ten factors, there would only be
449 more factors fragmented from the previous factor, with similar spectral profiles, but showed different
450 profile pattern with 510 – 560 Th in RCF2_D2 in Range Combined. The factorization of Range
451 Combined was mainly controlled by Range 1 and 2 due to high signals, and the signals in Range 3
452 are forced to be distributed according to the time series determined by Ranges 1 and 2. Ultimately,
453 this will lead to failure in factor separation for this low-signal range.
454 4.1.3 Nighttime factor comparison
455 Since high-mass dimers are more likely to form at night due to photochemical production of NO in
456 daytime, which inhibits RO_2 + RO_2 reactions, Range 3 had the highest fraction of nighttime signals
457 of all the sub-ranges. While Range 3 produced two nighttime factors, Ranges 2 and Combined showed
458 one, and Range 1 had no nighttime factor. The difference between the two results also indicates the
459 advantage of analyzing monomers and dimers separately.
460 The two nighttime factors in Range 3 can be clearly identified as arising from ozonolysis (R3F2_N1)
461 and a mix of ozonolysis and NO_3 oxidation (R3F2_N2) based on the mass spectral profiles, as
462 described above. The organonitrate at 555 Th, $C_{20}H_{31}O_{10}NO_3 \cdot NO_3^-$, is a typical marker for NO_3
463 radical initiated monoterpene chemistry (Yan et al., 2016). However, several interesting features
464 become evident when comparing to the results of Range 2 and Combined. Firstly, only one nighttime
465 factor (R2F4_N, RCF4_N) was separated in each of these ranges, and that shows clear resemblance
466 with ozonolysis of monoterpenes as measured in numerous studies, e.g. (Ehn et al., 2012;Ehn et al.,
467 2014). Secondly, the high correlation found in Figure 6b between the ozonolysis factors (i.e.,
468 R2F4_N, R3F2_N1, RCF4_N), further supports the assignment. However, this factor is the only
469 nighttime factor in the monomer range, suggesting that NO_3 radical chemistry of monoterpenes in
470 Hyytiälä does not form substantial amounts of HOM monomers. The only way for the CI-APi-TOF
471 to detect products of monoterpene-NO_3 radical chemistry may thus be through the dimers, where one

https://doi.org/10.5194/acp-2019-838
Preprint. Discussion started: 28 November 2019


Atmospheric Chemistry and Physics Discussions

highly oxygenated RO_2 radical from ozonolysis reacts with a less oxygenated RO_2 radical from NO_3 oxidation.

In the results by Yan et al. (2016) the combined UMR-PMF of monomers and dimers did yield a considerable amount of compounds in the monomer range also for the NO_3 radical chemistry factor. There may be several reasons for this discrepancy. One major cause for differences between the spring dataset of Yan et al. (2016) and the autumn dataset presented here, is that nighttime concentrations of HOM was greatly reduced during our autumn campaign. The cause may have been fairly frequent fog formation during nights, and also the concentration of e.g. ozone decreased nearly to zero during several nights (Zha et al., 2018). It is also possible that the NO_3 radical-related factor by Yan et al. (2016) is probably a mixture of NO_3 and O_3 radical chemistry, while the monomer may thus be attributed to the O_3 part. Alternatively, the different conditions during the two measurement periods, as well as seasonal difference in monoterpene mixtures (Hakola et al., 2012), caused variations in the oxidation pathways.

4.1.4 Contamination factor

During the campaign, an automated instrument zeroing every three hours was conducted, by switching a valve to pass the air through a HEPA filter. Each zeroing process lasted for 10 min. While the zeroing successfully removed the low-volatile HOM and H_2SO_4, the zeroing process introduced contaminants into the inlet lines. The contaminants were primarily different types of perfluorinated organic acids, often off-gassing from e.g. Teflon tubing. For IVOC contaminants, these would be flushed through the inlet, while (E)LVOC would condense onto the inlet walls and not come off. However, SVOC contaminants may stick to the inlet tubing and slowly evaporate back into the sampled air. We removed all the 10-min zeroing periods, and averaged the data to 1-h time resolution, but contaminants were still identified in all ranges by binPMF.

Contamination contributed 10%, 3%, 19% and 4% to Range 1, 2, 3, and Combined, respectively, in the binPMF solutions where the contamination factor was first separated. This also explains why the contamination factor was separated much earlier in Ranges 1 and 3 than in Range 2. However, despite contributing slightly more to Range Combined than to Range 2, the contamination factor was separated when the factor number was increased by one in Range Combined. Here, the difference in volatility of the contaminants in the different sub-ranges may play a role, such that the contaminants in different sub-ranges behave differently. Thus, the behavior of the contamination factor across the combined range is not consistent. Therefore, we examined the zeroing effect with finer time resolution, i.e. 1 min, with three of the largest fluorinated compounds in each range of our mass spectrum, $(CF_2)_3CO_2HF{\cdot}NO_3^-$ (275.9748 Th), $(CF_2)_5C_2O_4H^-$ (338.9721 Th), and $(CF_2)_6CO_2HF{\cdot}NO_3^-$ (425.9653 Th). Since the overall signal levels were very low for these compounds, the time series

https://doi.org/10.5194/acp-2019-838
Preprint. Discussion started: 28 November 2019

Atmospheric Chemistry and Physics Discussions

506 became very noisy with such high time resolution. This made it impossible to perform HR fitting for
507 the data, and instead we summed up the signal from the mass ranges where we expected unperturbed
508 signal from these ions.
509 The time series with sawtooth pattern of the three fluorinated compounds is shown in Figure S3 in
510 Supplement. From the time series, we selected a period of around three days of the 3-h cycles (25 in
511 total), and in Figure 7 the cycles were aligned and superimposed on top of one another, normalized
512 by the maximum during the zeroing. The normalized signals of the three compounds are shown in
513 light colors, and the mean values shown in bold sold lines. This data includes also the zeroing periods
514 to highlight the effect, but these periods were removed from the data used for our PMF analyses.

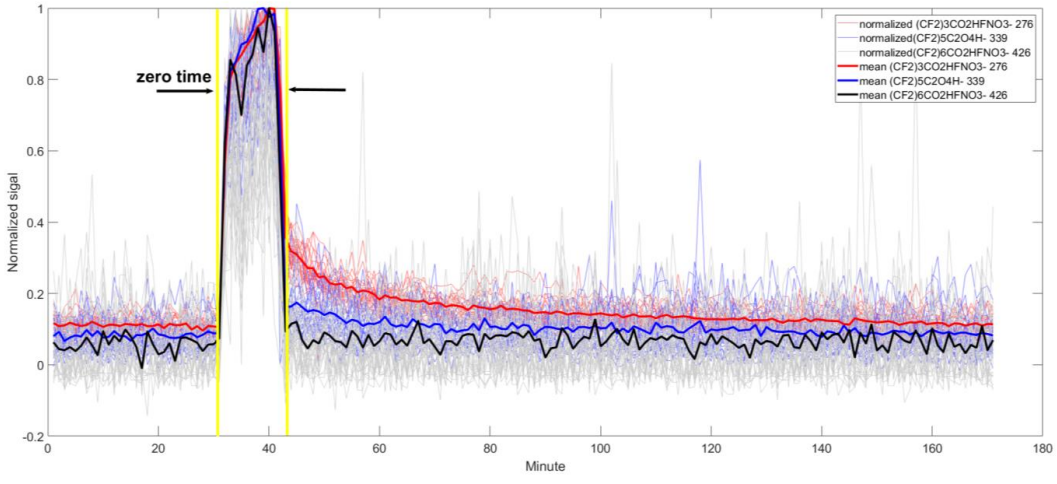

515

516 Figure 7 Normalized signals for three fluorinated compounds during a 3-h cycle (180 minutes), with
517 $(CF_2)_3CO_2HF{\cdot}NO_3^-$ (275.9748 Th) in red, $(CF_2)_5C_2O_4H^-$ (338.9721 Th) in blue, and
518 $(CF_2)_6CO_2HF{\cdot}NO_3^-$ (425.9653 Th) in black. We selected 25 cycles and normalized all the cycles by
519 their individual maximum. The yellow window shows the zeroing time, for around 10 minutes, which
520 has been removed from the data analysis. Light colors display the individual cycles, and the bold
521 solid colors stand for the average for each compounds.
522 The signals of the three fluorinated compounds increased by 10 to 20 times during the zeros, due to
523 off-gassing either in the filter or in the tubing in the zeroing setup. Immediately after the zeroing was
524 stopped, signals of all three compounds dropped by about 60-90%, followed by a gradual decay. The
525 decay period coincided with our ambient sampling, and therefore these signals are part of our dataset.
526 It is evident that the three fluorinated compounds were from the same source (zeroing process), but
527 due to their different volatilities, they were lost at different rates. This, in turn, means that the spectral
528 signature of this source will change as a function of time, at odds with one of the basic assumptions

https://doi.org/10.5194/acp-2019-838
Preprint. Discussion started: 28 November 2019

Atmospheric Chemistry and Physics Discussions

of PMF. Panels a and b in Figure S4 displays the temporal correlation with and without zeroing period with 1 min time resolution. The correlation coefficients dropped greatly when the zero period was removed, from 0.9 to 0.3 for R^2 between 276 Th and 339 Th, and 0.8 to 0.1 between 276 Th and 426 Th. Similar effect is also found with the 1 h averaged data (Fig. S4c, d).

This detailed analysis of fluorinated contamination in our system was here merely used as an example to show that volatility can impact source profiles over time. In this case, the contamination factor was still identified both from the separate sub-ranges and from the combined data set using binPMF. However, the contamination profile in the combined range is now averaged, compared to that from separate ranges: the fractional contributions of contamination compounds to this profile, vary during the process of each zeroing due to different volatility properties. In Figure S5, contamination factor profiles from Range 3 and Range Combined were compared. It can be clearly seen that the profile of Range Combined is more noisy than that of Range 3, probably due to the varied fractional contributions of contamination compounds to the profile. In ambient data, products from different sources can have undergone atmospheric processing, altering the product distribution. Our aim with this analysis was to highlight the importance of differences in the sink terms due to different volatilities of the products. This may be an important issue for gas phase mass spectrometry analysis, potentially underestimated by many PMF users, as it is likely only a minor issue for aerosol data, for which PMF has been applied much more routinely. If failing to achieve physically meaningful factors using PMF on gas phase mass spectra, our recommendation is to try applying PMF to sub-ranges of the spectrum, where IVOC, SVOC and (E)LVOC could be analyzed separately.

4.2 Atmospheric insights

While the previous section discussed several findings with atmospheric implications, we highlight two results below, which are particularly intriguing. We also include the correlation matrix of all PMF and factors and selected meteorological parameters in Table 2.

Table 2 Correlation between factors and meteorological parameters and gases

	R1F1_D1	R1F1_D2	R1F1_D3	R1F1_C	R2F1_D1	R2F2_D2	R2F3_D3	R2F4_N	R3F1_D	R3F2_N1	R3F3_N2	R3F4_C	RCF1_D1	RCF2_D2	RCF3_D3	RCF4_N
O_3	0.51	0.59	0.35	-0.18	0.47	0.57	0.36	0.43	0.55	0.33	0.27	0.22	0.49	0.57	0.33	0.34
NO	0.13	-0.01	0.24	-0.03	0.18	-0.02	0.24	-0.22	0.13	-0.19	-0.17	0.03	0.13	0.00	0.26	-0.18
NOx	-0.05	-0.22	-0.10	0.09	-0.01	-0.23	-0.11	-0.13	-0.16	-0.21	-0.04	0.04	-0.04	-0.22	-0.09	-0.11
RH	-0.46	-0.80	-0.63	0.30	-0.43	-0.82	-0.64	-0.27	-0.78	-0.39	-0.07	-0.07	-0.43	-0.82	-0.60	-0.21
T	0.66	0.72	0.40	-0.24	0.65	0.66	0.41	0.39	0.65	0.30	0.14	0.19	0.66	0.68	0.38	0.24
UVB	0.52	0.63	0.82	-0.40	0.52	0.68	0.84	-0.30	0.79	-0.08	-0.27	0.08	0.49	0.68	0.83	-0.29

https://doi.org/10.5194/acp-2019-838
Preprint. Discussion started: 28 November 2019


Atmospheric Chemistry and Physics Discussions

556 4.2.1 Daytime dimer formation

557 Dimers are primarily produced during nighttime, due to NO suppressing RO_2 + RO_2 reactions in
558 daytime (Ehn et al., 2014;Yan et al., 2016). However, in this study, we found one clear daytime factor
559 in Range 3 (R3F1_D, peak at local time 12:00, UTC+2) by sub-range analysis. With high loadings
560 from even masses including 516, 518, 520, 528, 540 Th, this only daytime factor in dimer range
561 correlated very well with two daytime factors in Ranges 1 and 2 (R1F2_D2, R1F3_D3, R2F2_D2,
562 R2F3_D3) (Figure 6b and c). Strong correlation between R3F1_D with solar radiation was found,
563 with R = 0.79 (Table 2). This may indicate involvement of OH oxidation in producing this factor.
564 As previous studies have shown, dimers greatly facilitate new particle formation (NPF) (Kirkby et
565 al., 2016;Troestl et al., 2016;Lehtipalo et al., 2018), and this daytime dimer factor may represent a
566 source of dimers that would impact the initial stages of NPF in Hyytiälä. Mohr et al. (2017) reported
567 a clear diel pattern of dimers (sum of about 60 dimeric compounds of $C_{16\text{-}20}H_{13\text{-}33}O_{6\text{-}9}$) during NPF
568 events in 2013 in Hyytiälä, with minimum at night and maximum after noon, and estimated these
569 dimers can contribute ~5% of the mass of sub-60 nm particles. The link between the dimers presented
570 in that paper and those reported here will require further studies, as will the proper quantification of
571 the dimer factor identified here.

572 4.2.2 Dimers initiated by NO_3 radicals

573 Previous studies show that NO_3 oxidation of α-pinene, the most abundant monoterpene in Hyytiälä
574 (Hakola et al., 2012), produces fairly little SOA mass (yields <4 %), while β-pinene shows yields of
575 up to 53 % (Bonn and Moorgat, 2002;Nah et al., 2016). The NO_3+β-pinene reaction results in low
576 volatile organic nitrate compounds with carboxylic acid, alcohol, and peroxide functional groups (Fry
577 et al., 2014;Boyd et al., 2015), while NO_3+α-pinene reaction will typically lose the nitrate functional
578 group and form oxidation products with high vapor pressures (Spittler et al., 2006;Perraud et al.,
579 2010). Most monoterpene-derived HOM, including monomers, are low-volatile (Peräkylä et al.,
580 2019) and thus a low SOA yield indicates a low HOM yield. Thus, while there are to our knowledge
581 no laboratory studies on HOM formation from NO_3 oxidation of α-pinene, a low yield can be expected
582 based on SOA studies.
583 As discussed in section 4.1.3, a dimer factor (R3F2_N2) was identified as a mix of ozonolysis and
584 NO_3 oxidation processes, dominated by the organonitrate at 555 Th, $C_{20}H_{31}O_{10}NO_3{\cdot}NO_3^-$. However,
585 unlike the pure ozonolysis dimer factor which had a corresponding monomer factor (R = 0.86 between
586 factor R2F4_N and R3 F2_N1), this NO_3-related dimer factor did not have an equivalent monomer
587 factor. This suggests that the NO_3 oxidation of the monoterpene mixture in Hyytiälä does not by itself
588 form much HOM, but in the presence of RO_2 from ozonolysis, the RO_2 from NO_3 oxidation can take
589 part in HOM dimer formation. This further implies that, different from previous knowledge based on

https://doi.org/10.5194/acp-2019-838
Preprint. Discussion started: 28 November 2019


Atmospheric Chemistry and Physics Discussions

single-oxidant experiments in chambers, NO_3 oxidation may have a larger impact on SOA formation in the atmosphere where different oxidants exist concurrently. This highlights the need for future laboratory studies to consider systems with multiple oxidants during monoterpene oxidation experiments, to truly understand the role and contribution of different oxidants, and NO_3 in particular.

5 Conclusions

The recent development in mass spectrometry has greatly improved the detection of atmospheric vapors and their oxidation products. Factor analysis, such as PMF, can reduce dimensionality of the big datasets and extract factors relating to different atmospheric pathways/sources. Optimally, PMF can link laboratory-generated spectra with ambient observations, significantly improving our understanding of complicated atmospheric processes. However, one of PMF's basic assumptions is that factor profiles remain constant in time, yet for atmospheric gas-phase species, varying sources, reactions and sinks may violate this assumption. Some of these variations are likely not addressable in the data analysis stage, but others may be. For example, molecules formed from the same source can have different temporal behaviors due to varying volatilities, and thus condense at different rates. Performing PMF separately with smaller ranges may circumvent this problem. By utilizing the newly presented binPMF approach, more variables can be extracted from a narrow mass range compared to traditional UMR PMF, while preserving more information in the spectrum.

We conducted separate binPMF analysis on three different sub-ranges to explore the potential benefits of such an approach for producing more physically meaningful factors. We utilized ambient data measured by CI-APi-TOF in a boreal forest environment, and selected sub-ranges from the mass spectrum that roughly corresponded to regions where we would expect the molecules to have similar volatilities and formation pathways. Selected ranges were Range 1 (250 – 300 Th), Range 2 (300 – 350 Th), and Range 3 (510 – 560 Th). binPMF was separately applied to these ranges, as well as to the combination of all three for comparison.

The different sub-ranges produced some similar and some different factors. First of all, volatility of species indeed affect the PMF results. We could clearly prove the benefit of sub-range binPMF using the contamination factor as an example. We found that different compounds emitted from the same source showed different temporal trends, likely due to differences in volatilities. This increased the difficulties for PMF to separate this source in the combined data set, and the resolved profile was still less accurate than in the analysis for the sub-ranges. We recommend that future studies of gas-phase mass spectra should pay attention to this volatility effect on factor analysis.

Secondly, chemistry or sources contributing to the particular range can be better separated. Only the binPMF analysis on Range 3, where HOM dimers are typically observed, resolved two nighttime

https://doi.org/10.5194/acp-2019-838
Preprint. Discussion started: 28 November 2019

Atmospheric Chemistry and Physics Discussions

factors, characterized by monoterpene oxidation related to NO_3 and O_3 oxidation. The monoterpene ozonolysis factor was separated from both Range 2 and 3, showing very good correlation between the ranges and mutually verifying the results.

Thirdly, peaks with smaller signal intensities can be correctly assigned. The signal intensities between different parts of the mass spectrum may vary by orders of magnitude. In the analysis of the combined range, the results were almost completely controlled by the higher signals from Range 1 and 2. The separate analysis on Range 3 allowed the low signals to provide important information, such as the NO_3 oxidation process. In addition, running binPMF on different separate mass ranges also allows us to compare the factors obtained from the different ranges and help to verify the results.

In addition, daytime dimer formation was identified, presumably initiated by OH/O_3 with a diurnal peak at around noon, which may contribute to NPF in Hyytiälä. Also, based on the sub-range binPMF analysis, we successfully separated NO_3–related dimers which did not have an equivalent monomer factor. The NO_3 related factor was consistent with earlier observations (Yan et al., 2016), but would not have been identified from this dataset without utilizing the different sub-ranges. In future laboratory experiments, more complex oxidation systems may be useful in order to understand the role NO_3 oxidation in SOA formation.

In summary, we identified several reasons to recommend PMF users to try running their analysis on selected sub-ranges in addition to the whole spectra. Ultimately, the approach should be study-goal dependent. In some cases the researcher wants a quick factor analysis to explore different features of their data, while in others more accurate and quantitative separation of different sources and atmospheric processes are needed. As binPMF and UMR-PMF both require very little data preparation, we expect that it in most cases will be worth the time for the analyst to test how PMF results look for a few selected sub-ranges of their mass spectra.

Data availability. The data used in this study are available from the first author upon request: please contact Yanjun Zhang (yanjun.zhang@helsinki.fi).

Author contributions. ME and YZ designed the study. QZ and MR collected the data; data analysis and manuscript writing were done by YZ. All coauthors discussed the results and commented the manuscript.

Competing interests. The authors declare that they have no conflict of interest

Acknowledgements. We thank the tofTools team for providing tools for mass spectrometry data analysis. The personnel of the Hyytiälä forestry field station are acknowledged for help during field measurements.

https://doi.org/10.5194/acp-2019-838
Preprint. Discussion started: 28 November 2019

Atmospheric Chemistry and Physics Discussions

Financial support. This research was supported by the European Research Council (Grant 638703-COALA), the Academy of Finland (grants 317380 and 320094), and the Vilho, Yrjö and Kalle Väisälä Foundation. K.R.D. acknowledges support by the Swiss National Science postdoc mobility grant P2EZP2_181599.

Reference

Äijälä, M., Heikkinen, L., Fröhlich, R., Canonaco, F., Prévôt, A. S. H., Junninen, H., Petäjä, T., Kulmala, M., Worsnop, D., and Ehn, M.: Resolving anthropogenic aerosol pollution types – deconvolution and exploratory classification of pollution events, Atmos. Chem. Phys., 17, 3165-3197, 10.5194/acp-17-3165-2017, 2017.

Allan, J. D., Jimenez, J. L., Williams, P. I., Alfarra, M. R., Bower, K. N., Jayne, J. T., Coe, H., and Worsnop, D. R.: Quantitative sampling using an Aerodyne aerosol mass spectrometer 1. Techniques of data interpretation and error analysis, Journal of Geophysical Research: Atmospheres, 108, 2003.

Atkinson, R., Aschmann, S. M., Arey, J., and Shorees, B.: Formation of OH radicals in the gas phase reactions of O3 with a series of terpenes, 97, 6065-6073, 10.1029/92jd00062, 1992.

Berndt, T., Mentler, B., Scholz, W., Fischer, L., Herrmann, H., Kulmala, M., and Hansel, A.: Accretion Product Formation from Ozonolysis and OH Radical Reaction of α-Pinene: Mechanistic Insight and the Influence of Isoprene and Ethylene, Environmental Science & Technology, 52, 11069-11077, 10.1021/acs.est.8b02210, 2018a.

Berndt, T., Scholz, W., Mentler, B., Fischer, L., Herrmann, H., Kulmala, M., and Hansel, A.: Accretion Product Formation from Self- and Cross-Reactions of RO2 Radicals in the Atmosphere, Angewandte Chemie International Edition in English 57, 3820-3824, 10.1002/anie.201710989, 2018b.

Bertram, T. H., Kimmel, J. R., Crisp, T. A., Ryder, O. S., Yatavelli, R. L. N., Thornton, J. A., Cubison, M. J., Gonin, M., and Worsnop, D. R.: A field-deployable, chemical ionization time-of-flight mass spectrometer, Atmospheric Measurement Techniques, 4, 1471-1479, 10.5194/amt-4-1471-2011, 2011.

Bianchi, F., Kurtén, T., Riva, M., Mohr, C., Rissanen, M. P., Roldin, P., Berndt, T., Crounse, J. D., Wennberg, P. O., Mentel, T. F., Wildt, J., Junninen, H., Jokinen, T., Kulmala, M., Worsnop, D. R., Thornton, J. A., Donahue, N., Kjaergaard, H. G., and Ehn, M.: Highly Oxygenated Organic Molecules (HOM) from Gas-Phase Autoxidation Involving Peroxy Radicals: A Key Contributor to Atmospheric Aerosol, Chemical Reviews, 119, 3472-3509, 10.1021/acs.chemrev.8b00395, 2019.

Bonn, B., and Moorgat, G. K.: New particle formation during a- and b-pinene oxidation by O3, OH and NO3, and the influence of water vapour: particle size distribution studies, Atmos. Chem. Phys., 2, 183-196, 10.5194/acp-2-183-2002, 2002.

Boyd, C. M., Sanchez, J., Xu, L., Eugene, A. J., Nah, T., Tuet, W. Y., Guzman, M. I., and Ng, N. L.: Secondary organic aerosol formation from the β-pinene+NO3 system: effect of humidity and peroxy radical fate, Atmos. Chem. Phys., 15, 7497-7522, 10.5194/acp-15-7497-2015, 2015.

Buchholz, A., Lambe, A. T., Ylisirniö, A., Li, Z., Tikkanen, O. P., Faiola, C., Kari, E., Hao, L., Luoma, O., Huang, W., Mohr, C., Worsnop, D. R., Nizkorodov, S. A., Yli-Juuti, T., Schobesberger, S., and Virtanen, A.: Insights into the O : C-dependent mechanisms controlling the evaporation of α-pinene secondary organic aerosol particles, Atmos. Chem. Phys., 19, 4061-4073, 10.5194/acp-19-4061-2019, 2019.

Canagaratna, M., Jayne, J., Jimenez, J., Allan, J., Alfarra, M., Zhang, Q., Onasch, T., Drewnick, F., Coe, H., and Middlebrook, A.: Chemical and microphysical characterization of ambient aerosols with the aerodyne aerosol mass spectrometer, Mass Spectrometry Reviews, 26, 185-222, 2007.

Canonaco, F., Crippa, M., Slowik, J., Baltensperger, U., and Prévôt, A.: SoFi, an IGOR-based interface for the efficient use of the generalized multilinear engine (ME-2) for the source apportionment: ME-2 application to aerosol mass spectrometer data, Atmospheric Measurement Techniques, 6, 3649, 2013.

Craven, J. S., Yee, L. D., Ng, N. L., Canagaratna, M. R., Loza, C. L., Schilling, K. A., Yatavelli, R. L. N., Thornton, J. A., Ziemann, P. J., Flagan, R. C., and Seinfeld, J. H.: Analysis of secondary organic aerosol formation and aging using positive matrix factorization of high-resolution aerosol mass spectra:

https://doi.org/10.5194/acp-2019-838
Preprint. Discussion started: 28 November 2019

application to the dodecane low-NO_x system, Atmos. Chem. Phys., 12, 11795-11817, 10.5194/acp-12-11795-2012, 2012.

Crippa, M., Canonaco, F., Lanz, V. A., Äijälä, M., Allan, J. D., Carbone, S., Capes, G., Ceburnis, D., Dall'Osto, M., Day, D. A., DeCarlo, P. F., Ehn, M., Eriksson, A., Freney, E., Hildebrandt Ruiz, L., Hillamo, R., Jimenez, J. L., Junninen, H., Kiendler-Scharr, A., Kortelainen, A. M., Kulmala, M., Laaksonen, A., Mensah, A. A., Mohr, C., Nemitz, E., O'Dowd, C., Ovadnevaite, J., Pandis, S. N., Petäjä, T., Poulain, L., Saarikoski, S., Sellegri, K., Swietlicki, E., Tiitta, P., Worsnop, D. R., Baltensperger, U., and Prévôt, A. S. H.: Organic aerosol components derived from 25 AMS data sets across Europe using a consistent ME-2 based source apportionment approach, Atmos. Chem. Phys., 14, 6159-6176, 10.5194/acp-14-6159-2014, 2014.

Ehn, M., Kleist, E., Junninen, H., Petäjä, T., Lönn, G., Schobesberger, S., Dal Maso, M., Trimborn, A., Kulmala, M., Worsnop, D. R., Wahner, A., Wildt, J., and Mentel, T. F.: Gas phase formation of extremely oxidized pinene reaction products in chamber and ambient air, Atmos. Chem. Phys., 12, 5113-5127, 10.5194/acp-12-5113-2012, 2012.

Ehn, M., Thornton, J. A., Kleist, E., Sipila, M., Junninen, H., Pullinen, I., Springer, M., Rubach, F., Tillmann, R., Lee, B., Lopez-Hilfiker, F., Andres, S., Acir, I.-H., Rissanen, M., Jokinen, T., Schobesberger, S., Kangasluoma, J., Kontkanen, J., Nieminen, T., Kurten, T., Nielsen, L. B., Jorgensen, S., Kjaergaard, H. G., Canagaratna, M., Dal Maso, M., Berndt, T., Petaja, T., Wahner, A., Kerminen, V.-M., Kulmala, M., Worsnop, D. R., Wildt, J., and Mentel, T. F.: A large source of low-volatility secondary organic aerosol, Nature, 506, 476-479, 10.1038/nature13032, 2014.

El Haddad, I., D'Anna, B., Temime-Roussel, B., Nicolas, M., Boreave, A., Favez, O., Voisin, D., Sciare, J., George, C., Jaffrezo, J. L., Wortham, H., and Marchand, N.: Towards a better understanding of the origins, chemical composition and aging of oxygenated organic aerosols: case study of a Mediterranean industrialized environment, Marseille, Atmos. Chem. Phys., 13, 7875-7894, 10.5194/acp-13-7875-2013, 2013.

Fry, J. L., Draper, D. C., Barsanti, K. C., Smith, J. N., Ortega, J., Winkler, P. M., Lawler, M. J., Brown, S. S., Edwards, P. M., Cohen, R. C., and Lee, L.: Secondary Organic Aerosol Formation and Organic Nitrate Yield from NO3 Oxidation of Biogenic Hydrocarbons, Environmental Science & Technology, 48, 11944-11953, 10.1021/es502204x, 2014.

Guenther, A., Hewitt, C. N., Erickson, D., Fall, R., Geron, C., Graedel, T., Harley, P., Klinger, L., Lerdau, M., McKay, W. A., Pierce, T., Scholes, B., Steinbrecher, R., Tallamraju, R., Taylor, J., and Zimmerman, P.: A GLOBAL-MODEL OF NATURAL VOLATILE ORGANIC-COMPOUND EMISSIONS, Journal of Geophysical Research-Atmospheres, 100, 8873-8892, 10.1029/94jd02950, 1995.

Hakola, H., Tarvainen, V., Bäck, J., Ranta, H., Bonn, B., Rinne, J., and Kulmala, M.: Seasonal variation of mono- and sesquiterpene emission rates of Scots pine, Biogeosciences, 3, 93-101, 10.5194/bg-3-93-2006, 2006.

Hakola, H., Hellén, H., Hemmilä, M., Rinne, J., and Kulmala, M.: In situ measurements of volatile organic compounds in a boreal forest, Atmos. Chem. Phys., 12, 11665-11678, 10.5194/acp-12-11665-2012, 2012.

Hari, P., and Kulmala, M.: Station for Measuring Ecosystem–Atmosphere Relations (SMEAR II), Boreal Environment Research, 10, 315-322, 2005.

Huang, S., Rahn, K. A., and Arimoto, R.: Testing and optimizing two factor-analysis techniques on aerosol at Narragansett, Rhode Island, Atmospheric Environment, 33, 2169-2185, https://doi.org/10.1016/S1352-2310(98)00324-0, 1999.

Huffman, J. A., Docherty, K. S., Aiken, A. C., Cubison, M. J., Ulbrich, I. M., DeCarlo, P. F., Sueper, D., Jayne, J. T., Worsnop, D. R., Ziemann, P. J., and Jimenez, J. L.: Chemically-resolved aerosol volatility measurements from two megacity field studies, Atmos. Chem. Phys., 9, 7161-7182, 10.5194/acp-9-7161-2009, 2009.

Jokinen, T., Sipilä, M., Junninen, H., Ehn, M., Lönn, G., Hakala, J., Petäjä, T., Mauldin Iii, R. L., Kulmala, M., and Worsnop, D. R.: Atmospheric sulphuric acid and neutral cluster measurements using CI-APi-TOF, Atmospheric Chemistry and Physics, 12, 4117-4125, 10.5194/acp-12-4117-2012, 2012.

Kirkby, J., Duplissy, J., Sengupta, K., Frege, C., Gordon, H., Williamson, C., Heinritzi, M., Simon, M., Yan, C., Almeida, J., Troestl, J., Nieminen, T., Ortega, I. K., Wagner, R., Adamov, A., Amorim, A., Bernhammer, A.-K., Bianchi, F., Breitenlechner, M., Brilke, S., Chen, X., Craven, J., Dias, A., Ehrhart, S., Flagan, R. C., Franchin, A., Fuchs, C., Guida, R., Hakala, J., Hoyle, C. R., Jokinen, T., Junninen, H., Kangasluoma, J., Kim, J., Krapf, M., Kuerten, A., Laaksonen, A., Lehtipalo, K., Makhmutov, V., Mathot,

https://doi.org/10.5194/acp-2019-838
Preprint. Discussion started: 28 November 2019

Atmospheric Chemistry and Physics Discussions

S., Molteni, U., Onnela, A., Peraekylae, O., Piel, F., Petaejae, T., Praplan, A. P., Pringle, K., Rap, A., Richards, N. A. D., Riipinen, I., Rissanen, M. P., Rondo, L., Sarnela, N., Schobesberger, S., Scott, C. E., Seinfeld, J. H., Sipilae, M., Steiner, G., Stozhkov, Y., Stratmann, F., Tome, A., Virtanen, A., Vogel, A. L., Wagner, A. C., Wagner, P. E., Weingartner, E., Wimmer, D., Winkler, P. M., Ye, P., Zhang, X., Hansel, A., Dommen, J., Donahue, N. M., Worsnop, D. R., Baltensperger, U., Kulmala, M., Carslaw, K. S., and Curtius, J.: Ion-induced nucleation of pure biogenic particles, Nature, 533, 521-526, 10.1038/nature17953, 2016.

Kulmala, M., Kontkanen, J., Junninen, H., Lehtipalo, K., Manninen, H. E., Nieminen, T., Petäjä, T., Sipilä, M., Schobesberger, S., Rantala, P., Franchin, A., Jokinen, T., Järvinen, E., Äijälä, M., Kangasluoma, J., Hakala, J., Aalto, P. P., Paasonen, P., Mikkilä, J., Vanhanen, J., Aalto, J., Hakola, H., Makkonen, U., Ruuskanen, T., Mauldin, R. L., Duplissy, J., Vehkamäki, H., Bäck, J., Kortelainen, A., Riipinen, I., Kurtén, T., Johnston, M. V., Smith, J. N., Ehn, M., Mentel, T. F., Lehtinen, K. E. J., Laaksonen, A., Kerminen, V.-M., and Worsnop, D. R.: Direct Observations of Atmospheric Aerosol Nucleation, 339, 943-946, 10.1126/science.1227385 %J Science, 2013.

Lamarque, J. F., Bond, T. C., Eyring, V., Granier, C., Heil, A., Klimont, Z., Lee, D., Liousse, C., Mieville, A., Owen, B., Schultz, M. G., Shindell, D., Smith, S. J., Stehfest, E., Van Aardenne, J., Cooper, O. R., Kainuma, M., Mahowald, N., McConnell, J. R., Naik, V., Riahi, K., and van Vuuren, D. P.: Historical (1850–2000) gridded anthropogenic and biomass burning emissions of reactive gases and aerosols: methodology and application, Atmos. Chem. Phys., 10, 7017-7039, 10.5194/acp-10-7017-2010, 2010.

Lee, B. H., Lopez-Hilfiker, F. D., Mohr, C., Kurtén, T., Worsnop, D. R., and Thornton, J. A.: An Iodide-Adduct High-Resolution Time-of-Flight Chemical-Ionization Mass Spectrometer: Application to Atmospheric Inorganic and Organic Compounds, Environmental Science & Technology, 48, 6309-6317, 10.1021/es500362a, 2014.

Lee, B. H., Lopez-Hilfiker, F. D., D'Ambro, E. L., Zhou, P., Boy, M., Petäjä, T., Hao, L., Virtanen, A., and Thornton, J. A.: Semi-volatile and highly oxygenated gaseous and particulate organic compounds observed above a boreal forest canopy, Atmos. Chem. Phys., 18, 11547-11562, 10.5194/acp-18-11547-2018, 2018.

Lehtipalo, K., Yan, C., Dada, L., Bianchi, F., Xiao, M., Wagner, R., Stolzenburg, D., Ahonen, L. R., Amorim, A., Baccarini, A., Bauer, P. S., Baumgartner, B., Bergen, A., Bernhammer, A.-K., Breitenlechner, M., Brilke, S., Buchholz, A., Mazon, S. B., Chen, D., Chen, X., Dias, A., Dommen, J., Draper, D. C., Duplissy, J., Ehn, M., Finkenzeller, H., Fischer, L., Frege, C., Fuchs, C., Garmash, O., Gordon, H., Hakala, J., He, X., Heikkinen, L., Heinritzi, M., Helm, J. C., Hofbauer, V., Hoyle, C. R., Jokinen, T., Kangasluoma, J., Kerminen, V.-M., Kim, C., Kirkby, J., Kontkanen, J., Kürten, A., Lawler, M. J., Mai, H., Mathot, S., Mauldin, R. L., Molteni, U., Nichman, L., Nie, W., Nieminen, T., Ojdanic, A., Onnela, A., Passananti, M., Petäjä, T., Piel, F., Pospisilova, V., Quéléver, L. L. J., Rissanen, M. P., Rose, C., Sarnela, N., Schallhart, S., Schuchmann, S., Sengupta, K., Simon, M., Sipilä, M., Tauber, C., Tomé, A., Tröstl, J., Väisänen, O., Vogel, A. L., Volkamer, R., Wagner, A. C., Wang, M., Weitz, L., Wimmer, D., Ye, P., Ylisirniö, A., Zha, Q., Carslaw, K. S., Curtius, J., Donahue, N. M., Flagan, R. C., Hansel, A., Riipinen, I., Virtanen, A., Winkler, P. M., Baltensperger, U., Kulmala, M., and Worsnop, D. R.: Multicomponent new particle formation from sulfuric acid, ammonia, and biogenic vapors, 4, eaau5363, 10.1126/sciadv.aau5363 %J Science Advances, 2018.

Liebmann, J., Karu, E., Sobanski, N., Schuladen, J., Ehn, M., Schallhart, S., Quéléver, L., Hellen, H., Hakola, H., Hoffmann, T., Williams, J., Fischer, H., Lelieveld, J., and Crowley, J. N.: Direct measurement of NO3 radical reactivity in a boreal forest, Atmos. Chem. Phys., 18, 3799-3815, 10.5194/acp-18-3799-2018, 2018.

Massoli, P., Stark, H., Canagaratna, M. R., Krechmer, J. E., Xu, L., Ng, N. L., Mauldin, R. L., Yan, C., Kimmel, J., Misztal, P. K., Jimenez, J. L., Jayne, J. T., and Worsnop, D. R.: Ambient Measurements of Highly Oxidized Gas-Phase Molecules during the Southern Oxidant and Aerosol Study (SOAS) 2013, ACS Earth and Space Chemistry, 10.1021/acsearthspacechem.8b00028, 2018.

Mohr, C., Lopez-Hilfiker, F. D., Yli-Juuti, T., Heitto, A., Lutz, A., Hallquist, M., D'Ambro, E. L., Rissanen, M. P., Hao, L., Schobesberger, S., Kulmala, M., Mauldin III, R. L., Makkonen, U., Sipilä, M., Petäjä, T., and Thornton, J. A.: Ambient observations of dimers from terpene oxidation in the gas phase: Implications for new particle formation and growth, 44, 2958-2966, 10.1002/2017gl072718, 2017.

Nah, T., Sanchez, J., Boyd, C. M., and Ng, N. L.: Photochemical Aging of α-pinene and β-pinene Secondary Organic Aerosol formed from Nitrate Radical Oxidation, Environmental Science & Technology, 50, 222-231, 10.1021/acs.est.5b04594, 2016.

https://doi.org/10.5194/acp-2019-838
Preprint. Discussion started: 28 November 2019

Atmospheric Chemistry and Physics Discussions

828 Orlando, J. J., and Tyndall, G. S.: Laboratory studies of organic peroxy radical chemistry: an overview with
829 emphasis on recent issues of atmospheric significance, J Chemical Society Reviews, 41, 6294-6317, 2012.
830 Paatero, P., and Tapper, U.: Positive matrix factorization: A non-negative factor model with optimal utilization
831 of error estimates of data values, Environmetrics, 5, 111-126, 1994.
832 Paatero, P.: Least squares formulation of robust non-negative factor analysis, Chemometrics and Intelligent
833 Laboratory Systems, 37, 23-35, https://doi.org/10.1016/S0169-7439(96)00044-5, 1997.
834 Paatero, P.: The Multilinear Engine—A Table-Driven, Least Squares Program for Solving Multilinear
835 Problems, Including the n-Way Parallel Factor Analysis Model, Journal of Computational and Graphical
836 Statistics, 8, 854-888, 10.1080/10618600.1999.10474853, 1999.
837 Paciga, A., Karnezi, E., Kostenidou, E., Hildebrandt, L., Psichoudaki, M., Engelhart, G. J., Lee, B. H., Crippa,
838 M., Prévôt, A. S. H., Baltensperger, U., and Pandis, S. N.: Volatility of organic aerosol and its components
839 in the megacity of Paris, Atmos. Chem. Phys., 16, 2013-2023, 10.5194/acp-16-2013-2016, 2016.
840 Paulson, S. E., and Orlando, J. J.: The reactions of ozone with alkenes: An important source of HOx in the
841 boundary layer, 23, 3727-3730, 10.1029/96gl03477, 1996.
842 Peräkylä, O., Riva, M., Heikkinen, L., Quéléver, L., Roldin, P., and Ehn, M.: Experimental investigation into
843 the volatilities of highly oxygenated organic molecules (HOM), Atmospheric Chemistry and Physics
844 Discussions, 2019, 1-28, 10.5194/acp-2019-620, 2019.
845 Perraud, V., Bruns, E. A., Ezell, M. J., Johnson, S. N., Greaves, J., and Finlayson-Pitts, B. J.: Identification of
846 Organic Nitrates in the NO3 Radical Initiated Oxidation of α-Pinene by Atmospheric Pressure Chemical
847 Ionization Mass Spectrometry, Environmental Science & Technology, 44, 5887-5893, 10.1021/es1005658,
848 2010.
849 Polissar, A. V., Hopke, P. K., Paatero, P., Malm, W. C., and Sisler, J. F.: Atmospheric aerosol over Alaska: 2.
850 Elemental composition and sources, Journal of Geophysical Research: Atmospheres, 103, 19045-19057,
851 1998.
852 Pope III, C. A., Ezzati, M., and Dockery, D. W.: Fine-particulate air pollution and life expectancy in the United
853 States, New England Journal of Medicine, 360, 376-386, 2009.
854 Riva, M., Rantala, P., Krechmer, J. E., Peräkylä, O., Zhang, Y., Heikkinen, L., Garmash, O., Yan, C., Kulmala,
855 M., Worsnop, D., and Ehn, M.: Evaluating the performance of five different chemical ionization
856 techniques for detecting gaseous oxygenated organic species, Atmospheric Measurement Techniques, 12,
857 2403-2421, 10.5194/amt-12-2403-2019, 2019.
858 Sekimoto, K., Koss, A. R., Gilman, J. B., Selimovic, V., Coggon, M. M., Zarzana, K. J., Yuan, B., Lerner, B.
859 M., Brown, S. S., Warneke, C., Yokelson, R. J., Roberts, J. M., and de Gouw, J.: High- and low-
860 temperature pyrolysis profiles describe volatile organic compound emissions from western US wildfire
861 fuels, Atmos. Chem. Phys., 18, 9263-9281, 10.5194/acp-18-9263-2018, 2018.
862 Shiraiwa, M., Ueda, K., Pozzer, A., Lammel, G., Kampf, C. J., Fushimi, A., Enami, S., Arangio, A. M.,
863 Fröhlich-Nowoisky, J., Fujitani, Y., Furuyama, A., Lakey, P. S. J., Lelieveld, J., Lucas, K., Morino, Y.,
864 Pöschl, U., Takahama, S., Takami, A., Tong, H., Weber, B., Yoshino, A., and Sato, K.: Aerosol Health
865 Effects from Molecular to Global Scales, Environmental Science & Technology, 51, 13545-13567,
866 10.1021/acs.est.7b04417, 2017.
867 Song, Y., Shao, M., Liu, Y., Lu, S., Kuster, W., Goldan, P., and Xie, S.: Source apportionment of ambient
868 volatile organic compounds in Beijing, Environmental science & technology, 41, 4348-4353, 2007.
869 Spittler, M., Barnes, I., Bejan, I., Brockmann, K. J., Benter, T., and Wirtz, K.: Reactions of NO3 radicals with
870 limonene and α-pinene: Product and SOA formation, Atmospheric Environment, 40, 116-127,
871 https://doi.org/10.1016/j.atmosenv.2005.09.093, 2006.
872 Stocker, T., Qin, D., Plattner, G., Tignor, M., Allen, S., Boschung, J., Nauels, A., Xia, Y., Bex, V., and Midgley,
873 P.: IPCC, 2013: Climate Change 2013: The Physical Science Basis. Contribution of Working Group I to
874 the Fifth Assessment Report of the Intergovernmental Panel on Climate Change, 1535 pp, in, Cambridge
875 Univ. Press, Cambridge, UK, and New York, 2013.
876 Troestl, J., Chuang, W. K., Gordon, H., Heinritzi, M., Yan, C., Molteni, U., Ahlm, L., Frege, C., Bianchi, F.,
877 Wagner, R., Simon, M., Lehtipalo, K., Williamson, C., Craven, J. S., Duplissy, J., Adamov, A., Almeida,
878 J., Bernhammer, A.-K., Breitenlechner, M., Brilke, S., Dias, A., Ehrhart, S., Flagan, R. C., Franchin, A.,
879 Fuchs, C., Guida, R., Gysel, M., Hansel, A., Hoyle, C. R., Jokinen, T., Junninen, H., Kangasluoma, J.,
880 Keskinen, H., Kim, J., Krapf, M., Kuerten, A., Laaksonen, A., Lawler, M., Leiminger, M., Mathot, S.,
881 Moehler, O., Nieminen, T., Onnela, A., Petaejae, T., Piel, F. M., Miettinen, P., Rissanen, M. P., Rondo,
882 L., Sarnela, N., Schobesberger, S., Sengupta, K., Sipila, M., Smith, J. N., Steiner, G., Tome, A., Virtanen,

https://doi.org/10.5194/acp-2019-838
Preprint. Discussion started: 28 November 2019

Atmospheric Chemistry and Physics Discussions

A., Wagner, A. C., Weingartner, E., Wimmer, D., Winkler, P. M., Ye, P., Carslaw, K. S., Curtius, J., Dommen, J., Kirkby, J., Kulmala, M., Riipinen, I., Worsnop, D. R., Donahue, N. M., and Baltensperger, U.: The role of low-volatility organic compounds in initial particle growth in the atmosphere, Nature, 533, 527-531, 10.1038/nature18271, 2016.

Ulbrich, I. M., Canagaratna, M. R., Zhang, Q., Worsnop, D. R., and Jimenez, J. L.: Interpretation of organic components from Positive Matrix Factorization of aerosol mass spectrometric data, Atmos. Chem. Phys., 9, 2891-2918, 10.5194/acp-9-2891-2009, 2009.

Yan, C., Nie, W., Aijala, M., Rissanen, M. P., Canagaratna, M. R., Massoli, P., Junninen, H., Jokinen, T., Sarnela, N., Hame, S. A. K., Schobesberger, S., Canonaco, F., Yao, L., Prevot, A. S. H., Petaja, T., Kulmala, M., Sipila, M., Worsnop, D. R., and Ehn, M.: Source characterization of highly oxidized multifunctional compounds in a boreal forest environment using positive matrix factorization, Atmospheric Chemistry and Physics, 16, 12715-12731, 10.5194/acp-16-12715-2016, 2016.

Zha, Q., Yan, C., Junninen, H., Riva, M., Sarnela, N., Aalto, J., Quéléver, L., Schallhart, S., Dada, L., Heikkinen, L., Peräkylä, O., Zou, J., Rose, C., Wang, Y., Mammarella, I., Katul, G., Vesala, T., Worsnop, D. R., Kulmala, M., Petäjä, T., Bianchi, F., and Ehn, M.: Vertical characterization of highly oxygenated molecules (HOMs) below and above a boreal forest canopy, Atmos. Chem. Phys., 18, 17437-17450, 10.5194/acp-18-17437-2018, 2018.

Zhang, Q., Jimenez, J. L., Canagaratna, M. R., Ulbrich, I. M., Ng, N. L., Worsnop, D. R., and Sun, Y.: Understanding atmospheric organic aerosols via factor analysis of aerosol mass spectrometry: a review, Analytical and Bioanalytical Chemistry, 401, 3045-3067, 10.1007/s00216-011-5355-y, 2011.

Zhang, Y., Lin, Y., Cai, J., Liu, Y., Hong, L., Qin, M., Zhao, Y., Ma, J., Wang, X., and Zhu, T.: Atmospheric PAHs in North China: spatial distribution and sources, Science of the Total Environment, 565, 994-1000, 2016.

Zhang, Y., Cai, J., Wang, S., He, K., and Zheng, M.: Review of receptor-based source apportionment research of fine particulate matter and its challenges in China, Science of the Total Environment, 586, 917-929, 2017.

Zhang, Y., Peräkylä, O., Yan, C., Heikkinen, L., Äijälä, M., Daellenbach, K. R., Zha, Q., Riva, M., Garmash, O., Junninen, H., Paatero, P., Worsnop, D., and Ehn, M.: A novel approach for simple statistical analysis of high-resolution mass spectra, Atmospheric Measurement Techniques, 12, 3761-3776, 10.5194/amt-12-3761-2019, 2019.